The minimum energy necessary for escape is $E_f+e\phi$ or, in aluminum, 15.9 eV. Electrons excited from near the Fermi energy by absorpton of photons with $h\nu=9.18$ eV have an energy of nearly 20.9 eV. The escape cone for these electrons is easily determined and is found to be approximately 0.26π.

The escape cone for Table IV is not much less than 0.26π. By interpolating between Tables III and IV, it is seen that the escape probability is tatisfied by mean free paths between $l_p=100$ Å, $l_e=600$ Å and $l_p=250$ Å, $l_e=1000$ Å. Because α^{-1} for aluminum is 67 Å while the tables were constructed for $\alpha^{-1}=100$ Å, it is necessary to scale the results. Thus, for electrons in aluminum, which are about 9 eV above the Fermi energy, the mean free paths are between $l_p=67$ Å, $l_e=400$ Å and $l_p=167$ Å, $l_e=667$ Å. This just spans the values $l_p=130$ Å, $l_e=510$ Å which were found to give the best fit when a detailed analysis was made of the entire energy distribution of electrons emitted from aluminum.[9] It should be noted, though, that Quinn's theoretical calculation of l_e in aluminum[13] indicates a value of about 50 Å for electrons of energy greater than 5 eV above the Fermi energy, and appears to be in substantial disagreement with our analysis of the experimental results.

[13] J. J. Quinn, Phys. Rev. **126**, 1453 (1962).

PHYSICAL REVIEW VOLUME 156, NUMBER 2 10 APRIL 1967

Properties of the Mn^{55} Nuclear-Magnetic-Resonance Modes in $CsMnF_3$†

L. B. WELSH*
Department of Physics, University of California, Berkeley, California
(Received 20 June 1966)

A new NMR mode of the Mn^{55} nuclei in the hexagonal antiferromagnet $CsMnF_3$ has been observed directly between 673 and 676 Mc/sec. This mode results from the difference in the hyperfine couplings for nuclei of the Mn1 and Mn2 sites when the nuclei are strongly coupled by the Suhl-Nakamura (SN) interaction. The new NMR mode resembles an antiferromagnetic (AFM) exchange mode, while the NMR mode observed by Minkiewicz resembles an acoustic AFM mode. The linewidths of the acoustic and exchange NMR modes at 5000 Oe are 0.042 and 0.22 Mc/sec, respectively. These are a factor of ten narrower than predicted from the SN interaction. A four-sublattice model of $CsMnF_3$ is proposed which accounts for the field dependence of both NMR modes. The NMR frequencies extrapolated to infinite nuclear temperature are 666.0 ± 0.2 Mc/sec for the Mn2 site and 676.85 ± 0.1 Mc/sec for the Mn1 site. This suggests zero-point spin-wave reductions of $(2.2\pm1.0)\%$ and $(3.2\pm1.0)\%$ for the Mn1 and Mn2 sites; Davis's calculation predicts 2.49% and 4.36%, respectively. The temperature dependence of the electron-sublattice magnetization is determined from the temperature dependence of the exchange NMR mode. Four-sublattice-model spin-wave calculations account for this temperature dependence when an intrasublattice ferromagnetic exchange energy is included which is 32% of the antiferromagnetic intersublattice exchange energy. The Mn^{55} nuclear spin-lattice relaxation times have been determined for fields between 600 and 5000 Oe and for temperatures between 1.4 and 4.2°K. The field dependence and magnitude of the relaxation times are not understood, but at 5000 Oe, $T_1\propto T^{-4.96\pm0.03}$ with T_1 equal to 3.7 sec at 1.4°K. This temperature dependence indicates that three-magnon processes may be responsible for the relaxation.

I. INTRODUCTION

THE magnetic properties of the hexagonal antiferromagnet $CsMnF_3$ have been the subject of several previous studies. Torsion measurements, susceptibility measurements, antiferromagnetic resonance (AFR) studies, and electron-nuclear double-resonance studies have been performed by Lee *et al.*[1] Witt and Portis used the method of electron-nuclear double resonance to measure the Mn^{55} nuclear spin-lattice relaxation time[2] and to investigate the diffusion of energy in the nuclear spin system.[3] Minkiewicz and Nakamura[4] studied the Mn^{55} nuclear magnetic resonance (NMR) directly.

In Sec. II we discuss the direct observation of a second Mn^{55} nuclear resonance mode in $CsMnF_3$. A four-sublattice model for $CsMnF_3$ is described which accounts for the observed behavior of both NMR modes. For the two inequivalent Mn^{2+} sites the hyperfine coupling constants and the zero-point spin reductions are determined and compared with theory. From

† Supported by the U. S. Atomic Energy Commission through Contract AT(11-1)-34 Project 47. Report Code UCB-34P47-2.
* Present address: Department of Physics, University of Pennsylvania, Philadelphia, Pennsylvania.
[1] K. Lee, A. M. Portis, and G. L. Witt, Phys. Rev. **132**, 144 (1963).
[2] G. L. Witt and A. M. Portis, Phys. Rev. **136**, A136 (1964).
[3] G. L. Witt, thesis, University of California, 1964 (unpublished).
[4] V. Minkiewicz and A. Nakamura, Phys. Rev. **143**, 361 (1966).

the temperature dependence of the exchange-like NMR mode, we determine the temperature dependence of the sublattice magnetization.

In Sec. III a spin-wave calculation is described which is based on the four-sublattice model of Sec. II. This spin-wave calculation can account for the observed temperature dependence of the sublattice magnetization when ferromagnetic intrasublattice exchange is included. Agreement is obtained when this exchange is equal to 32% of the intersublattice antiferromagnetic exchange.

In Sec. IV we describe direct measurements of the Mn^{55} nuclear spin-lattice relaxation times. The temperature dependence of these relaxation times indicates that three magnon processes are responsible for the nuclear spin-lattice relaxation.

II. NUCLEAR-RESONANCE MODES IN $CsMnF_3$

Structure

The crystal structure of $CsMnF_3$ is the same as the hexagonal form of $BaTiO_3$.[5] Figure 1 shows one-half of the unit cell. The unit cell has the dimensions $a=6.213 \pm 0.003$ Å and $c=15.074 \pm 0.004$ Å. The space group $P6_3/mmc$. The full unit cell contains six formula weights. One-third of the manganese sites (denoted Mn1) are surrounded by fluorines having one type of distortion. The other two-thirds of the manganese sites (denoted Mn2) are surrounded by fluorines having two different distortions. The Mn1 sites have the point symmetry $\bar{3}m$ (D_{3d}) and have six nearest neighbors of type Mn2. The Mn2 sites have the point symmetry $3m$ (C_{3v}) with three nearest neighbors of type Mn1 and one type Mn2. Within the basal plane each site has six next-nearest neighbors of the same type.

The orientation of the electron spins is determined by a strong uniaxial anisotropy which makes the basal plane an easy plane. Anisotropy in the basal plane is essentially zero,[1,4] the preferred direction of the spins being established when external fields are applied. As a result, the electron spins are always perpendicular to the applied field regardless of the direction in which the field is applied (i.e., the spin-flop field is zero). The electron spins lie perpendicular to the hexagonal c axis in ferromagnetic planes. These ferromagnetic planes are stacked antiferromagnetically along the c axis. Each ferromagnetic plane contains only one type of Mn^{55} site. The stacking along the c axis may be denoted by $A(+)$, $B(-)$, $B(+)$, $A(-)$, $C(+)$, $C(-)$, $A(+)$, where $(+)$ and $(-)$ refer to the electron spin direction in space, A refers to an Mn1 type of ferromagnetic plane, and B and C refer to Mn2 type ferromagnetic planes.

Because of the lack of in-plane anisotropy, $CsMnF_3$ has one low-frequency AFR mode which is observable

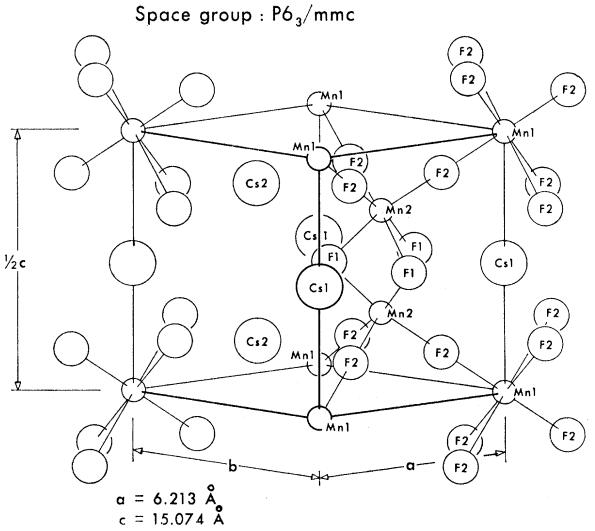

FIG. 1. Half of the chemical cell of $CsMnF_3$.

at X-band frequencies. The behaviors of this AFR mode and the MNR modes are strikingly altered by the coupling of the electrons and the nuclei through the hyperfine interaction $-\alpha \mathbf{m} \cdot \mathbf{M}$, where $\mathbf{m}$ refers to the nuclear magnetization and $\mathbf{M}$ refers to the electronic magnetization. De Gennes *et al.*[6] have discussed this effect in some detail for both ferromagnets and antiferromagnets. In terms of a two-sublattice model for $CsMnF_3$[1] the NMR frequency is altered to

$$\omega^2=(\gamma\alpha M)^2(1-\Gamma^2 2H_E\alpha m/\Omega_1^2), \quad (1)$$

where the low-frequency AFR mode is given by

$$\Omega_1^2=\Gamma^2(H^2+2H_E\alpha m), \quad (2)$$

and H_E is the exchange field, H the applied field, γ the nuclear gyromagnetic ratio, and Γ the electronic gyromagnetic ratio. These coupling effects are also present in $KMnF_3$,[7] $RbMnF_3$,[8] and $MnCO_3$[9] but are less pronounced.

Four-Sublattice Model of $CsMnF_3$

In this section we wish to consider a general four-sublattice model of $CsMnF_3$ which will be valid for calculations involving uniform-mode resonances and long-wavelength spin waves. The unit cell contains six different ferromagnetic planes. The sites on planes $A(+)$ and $A(-)$ possess inversion symmetry. The sites on $B(+)$ are related to the sites on $C(+)$ by inversion symmetry. The same relation holds between the sites on the $B(-)$ and $C(-)$ planes. From the four planes $B(+)$, $C(+)$, $B(-)$, and $C(-)$, two planes can be

[5] A. Zalkin, K. Lee, and D. H. Templeton, J. Chem. Phys. **37**, 697 (1962).

[6] P. G. de Gennes, P. A. Pincus, F. Hartmann-Boutron, and J. M. Winter, Phys. Rev. **129**, 1105 (1963).

[7] V. Minkiewicz and A. Nakamura, Phys. Rev. **143**, 365 (1966).

[8] A. J. Heeger and D. T. Teaney, J. Appl. Phys. Suppl. **35**, 846 (1964).

[9] H. J. Fink and D. Shaltiel, Phys. Rev. **136**, A218 (1964).

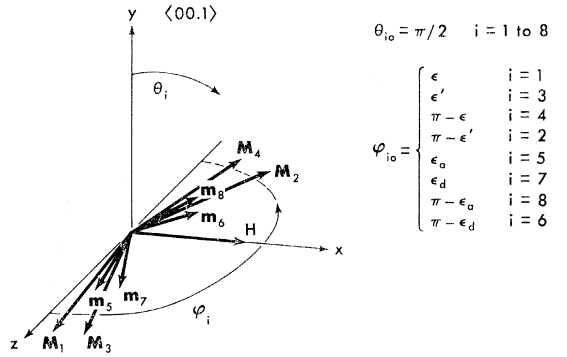

FIG. 2. Coordinate system and equilibrium positions of the electronic and nuclear magnetizations for the four-sublattice model of $CsMnF_3$. The magnetic field is applied in the basal plane.

constructed which have the average properties of the original planes. Planes $B(+)$ and $C(+)$ are added together to form one $(+)$ sublattice and planes $B(-)$ and $C(-)$ are added together to form one $(-)$ sublattice. The resulting sublattices $D(+)$ and $D(-)$ contain twice the number of magnetic ions of the sublattices $A(+)$ and $A(-)$. The properties of the sublattices $D(+)$ and $D(-)$ will be the average properties of planes $B(+)$, $C(+)$ and $B(-)$, $C(-)$ which implies the new sublattices also possess inversion symmetry.

The exchange interactions between the ferromagnetic planes are antiferromagnetic. The strength of the Mn1–Mn2 exchange interaction is measured by the exchange constant λ_1' and the Mn2-Mn2 exchange interaction by λ_2'. In terms of the sublattice mangetizations the total isotropic exchange energy for the original six planes is

$$U_{ex}=\lambda_1'\mathbf{M}_{A(+)}\cdot(\mathbf{M}_{B(-)}+\mathbf{M}_{C(-)})+\lambda_2'\mathbf{M}_{B(-)}\cdot\mathbf{M}_{B(+)} +\lambda_1'\mathbf{M}_{A(-)}\cdot(\mathbf{M}_{C(+)}+\mathbf{M}_{B(+)})+\lambda_2'\mathbf{M}_{C(+)}\cdot\mathbf{M}_{C(-)}. \quad (3)$$

Equation (3) reduces to

$$U_{ex}=\lambda_1(\mathbf{M}_{A(+)}\cdot\mathbf{M}_{D(-)}+\mathbf{M}_{A(-)}\cdot\mathbf{M}_{D(+)}) +\lambda_2(\mathbf{M}_{D(-)}\cdot\mathbf{M}_{D(+)}), \quad (4)$$

where $\lambda_1=2\lambda_1'$ and $\lambda_2=2\lambda_2'$. The magnetizations $\mathbf{M}_{D(-)}$ and $\mathbf{M}_{D(+)}$ are one-half the actual D-sublattice magnetization.

The total energy of the magnetic system is

$$U=\lambda_1(\mathbf{M}_1\cdot\mathbf{M}_2+\mathbf{M}_3\cdot\mathbf{M}_4)+\lambda_2\mathbf{M}_2\cdot\mathbf{M}_3 -\mathbf{H}\cdot(\mathbf{M}_1+2\mathbf{M}_2+2\mathbf{M}_3+\mathbf{M}_4)+(K/M^2) \times(M_{1y}^2+2M_{2y}^2+2M_{3y}^2+M_{4y}^2) -\mathbf{H}\cdot(\mathbf{m}_5+2\mathbf{m}_6+2\mathbf{m}_7+\mathbf{m}_8)-\alpha_a\mathbf{M}_1\cdot\mathbf{m}_5-2\alpha_d\mathbf{M}_2\cdot\mathbf{m}_6 -2\alpha_d\mathbf{M}_3\cdot\mathbf{m}_7-\alpha_a\mathbf{M}_4\cdot\mathbf{m}_8. \quad (5)$$

The sublattice notations are $A(+)\rightarrow 1$, $D(-)\rightarrow 2$, $D(+)\rightarrow 3$, $A(-)\rightarrow 4$. The parameters λ_1, λ_2, K, α_a, and α_d are positive; K is the anisotropy constant; α_a and α_d are the respective hyperfine interaction constants between the electron and nuclear magnetizations for the Mn1 and Mn2 sites. With the magnetic field applied in the basal plane, the sublattice magnetizations take the orientations shown in Fig. 2.

The equilibrium positions of the electron magnetizations are in the basal plane. These positions are determined by setting the first derivatives of the total energy with respect to the polar coordinate angles θ_i and φ_i equal to zero. The $\mathbf{M}_1$ and $\mathbf{M}_4$ sublattice magnetizations are tilted through an angle ϵ toward the applied field, and the magnetizations $\mathbf{M}_2$ and $\mathbf{M}_3$ are tilted toward the field through an angle ϵ' where these angles are given by

$$\epsilon\approx(2\lambda_2-\lambda_1)H/(2\lambda_1\lambda_2M), \quad \epsilon'\approx H/(2\lambda_2M). \quad (6)$$

Note that if $\lambda_2=\lambda_1$, then $\epsilon'=\epsilon$ and all sublattice magnetizations are tilted toward the field by the same amount. The equilibrium positions for the nuclei are $\epsilon_a=\epsilon+H/(\alpha_aM)$ for the nuclear magnetizations $\mathbf{m}_5$ and $\mathbf{m}_8$, and $\epsilon_d=\epsilon'+H/(\alpha_dM)$ for $\mathbf{m}_6$ and $\mathbf{m}_7$.

Minkiewicz and Nakamura[4] pointed out that the presence of two inequivalent Mn^{55} sites introduces a second NMR mode. This second NMR mode always lies above the mode which they observed and is only slightly depressed in frequency as a result of the coupling between the electron and nuclear modes. The AFR and NMR frequencies can be calculated from Eq. (5). In order to do this we make the assumption that all AFR frequencies are much larger than the NMR frequencies. In this case the nuclear spins will not respond to the AFR frequencies. The electron spins will only feel the average value of the nuclear magnetization. This reduces the effect of the hyperfine interaction to that of an effective nuclear-induced anisotropy field on the electron spins. This field acts in the equilibrium directions of the nuclear spins.

In order to calculate the AFR frequencies, Eq. (5) is treated in polar coordinates where the polar axis is chosen as the hexagonal c axis. Equation (5) is expanded to second order in the angular deviations $\delta\theta_i$ and $\delta\varphi_i$ about the equilibrium positions θ_{i0} and φ_{i0}. The first-order terms in $\delta\theta_i$ and $\delta\varphi_i$ vanish as a result of the equilibrium conditions. The resonance matrix from which the secular equation is obtained is calculated from the equations of motion in polar coordinate form. For sublattices 1 and 4 these are

$$\frac{\partial\delta\theta_i}{\partial t}=\frac{\Gamma}{M}\frac{\partial U}{\partial\delta\varphi_i}, \quad \frac{\partial\delta\varphi_i}{\partial t}=-\frac{\Gamma}{M}\frac{\partial U}{\partial\delta\theta_i}, \quad i=1,4. \quad (7)$$

For sublattices 2 and 3 the equations of motion are

$$\frac{\partial\delta\theta_i}{\partial t}=\frac{\Gamma}{2M}\frac{\partial U}{\partial\delta\varphi_i}, \quad \frac{\partial\delta\varphi_i}{\partial t}=-\frac{\Gamma}{2M}\frac{\partial U}{\partial\delta\theta_i}, \quad i=2,3. \quad (8)$$

The four resulting AFR modes are

$$\Omega_1^2=\Gamma^2(H^2+2H_EH_{AT}), \tag{9}$$

$$\Omega_2^2=\Gamma^2(2H_EH_A+2H_EH_{AT}-3H^2/4), \tag{10}$$

$$\Omega_3^2\approx 3\Gamma^2H_E^2/4, \tag{11}$$

$$\Omega_4^2\approx 3\Gamma^2H_E^2/4, \tag{12}$$

where $H_E=\lambda M$, $H_A=2K/M=7500$ Oe, and $H_{AT}=(\alpha_a+2\alpha_d)M/3=9.15/T_N$ Oe. The first-two modes are similar to those obtained by Lee *et al.*[1] using a simple two-sublattice model. The last two modes are high-frequency exchange modes.

The NMR frequencies are obtained by assuming the electron spins can follow adiabatically fields which vary at the NMR frequencies. From the full-equilibrium conditions for the electron spins we have

$$\frac{\partial U}{\partial\delta\theta_i}=0, \quad \frac{\partial U}{\partial\delta\varphi_i}=0, \quad i=1, 2, 3, 4. \tag{13}$$

The electron angular deviations can be determined as functions of the nuclear angular deviations $\delta\theta_i$ and $\delta\varphi_i$ where $i=5$ to 8. Using these relations, Eq. (5) may be expressed entirely in terms of the nuclear angular deviations. The resonance matrix for the NMR modes is then obtained from the equations of motion which are given by

$$\frac{\partial\delta\theta_i}{\partial t}=\frac{\gamma}{m_a}\frac{\partial U}{\partial\delta\varphi_i}, \quad \frac{\partial\delta\varphi_i}{\partial t}=-\frac{\gamma}{m_a}\frac{\partial U}{\partial\delta\theta_i}, \quad i=5, 8 \tag{14}$$

$$\frac{\partial\delta\theta_i}{\partial t}=\frac{\gamma}{2m_d}\frac{\partial U}{\partial\delta\varphi_i}, \quad \frac{\partial\delta\varphi_i}{\partial t}=-\frac{\gamma}{2m_d}\frac{\partial U}{\partial\delta\theta_i}, \quad i=6, 7. \tag{15}$$

Four NMR solutions result which are coupled together in pairs. The solutions of interest are given by

$$\begin{aligned}&\omega_1^2\omega_2^2=\omega_a^2\omega_d^2[1-\Gamma^2(4H_{AT_d}+2H_{AT_a})H_E/3\Omega_1^2],\\ &\omega_1^2+\omega_2^2=\omega_a^2(1-2\Gamma^2H_{AT_a}H_E/3\Omega_1^2)\\ &\qquad\qquad +\omega_d^2(1-4\Gamma^2H_{AT_d}H_E/3\Omega_1^2),\end{aligned} \tag{16}$$

where $\omega_a=\gamma\alpha_aM$, $\omega_d=\gamma\alpha_dM$, $H_{AT_a}=\alpha_am_a$, $H_{AT_d}=\alpha_dm_d$. The other pair of solutions involves Ω_2 and shows negligible coupling effects.

The behavior of the two solutions ω_1 and ω_2 is quite different. The lower solution, ω_1, exhibits the same behavior as the NMR mode obtained from the simple two-sublattice model and corresponds to the NMR mode observed by Minkiewicz and Nakamura.[4] The upper solution, ω_2, is only slightly depressed in frequency from the value ω_a and ω_d.

Using the resonance matrix of the nuclei which is generated by Eqs. (14) and (15), the relative normal-mode amplitudes of the nuclear magnetizations for the solutions ω_1 and ω_2 can be determined. Assuming $\Omega_1^2\gg\omega^2$, where ω satisfies Eq. (16), the relative normal-mode amplitudes are given by

$$\delta\varphi_5=\delta\varphi_8, \quad \delta\varphi_6=\delta\varphi_7, \quad \delta\theta_5=\delta\theta_8, \quad \delta\theta_6=\delta\theta_7,$$

$$\frac{\delta\varphi_7}{\delta\varphi_5}=\frac{\delta\theta_7}{\delta\theta_5}\approx\frac{\omega^2-\omega_a^2}{\omega^2-\omega_d^2}, \quad \delta\theta_5\approx i\frac{\omega_a}{\omega}\delta\varphi_5. \tag{17}$$

When $\omega=\omega_1$, the nuclear magnetizations $\mathbf{m}_5$ and $\mathbf{m}_8$ are in phase with $\mathbf{m}_6$ and $\mathbf{m}_7$, giving a net oscillating moment per unit cell which is the sum of the individual oscillating moments. When $\omega=\omega_2$, however, the $\mathbf{m}_5$ and $\mathbf{m}_8$ magnetizations are 180° out of phase with $\mathbf{m}_6$ and $\mathbf{m}_7$ as shown in Fig. 3 The oscillations of $\mathbf{m}_6$ and $\mathbf{m}_7$ nearly cancel those of $\mathbf{m}_5$ and $\mathbf{m}_8$ in this region as shown below. This produces a much smaller net oscillating moment per unit cell, which results in a large reduction in the net power absorbed from an rf field. Since the magnetizations oscillate in phase in the region where $\omega=\omega_1$, the lower mode resembles an acoustic electron spin-wave mode. The upper mode, where $\omega=\omega_2$, resembles an electron spin-wave *exchange mode* in that neighboring magnetizations oscillate out of phase. De Gennes[6] has pointed out that nuclear spin waves are well defined excitations at low temperatures when the electron and nuclear modes are strongly coupled. This coupling results in nuclear spin-wave dispersion relations which are depressed in frequency only for long wavelengths. The dispersion relation of the low NMR mode resembles the dispersion relation for the acoustic branch of the electron spin-wave spectrum, and the dispersion relation for the upper mode resembles that of the exchange branch of the electron spin-wave spectrum. In what follows, these two modes will be referred to as the *acoustic* and *exchange* NMR modes.

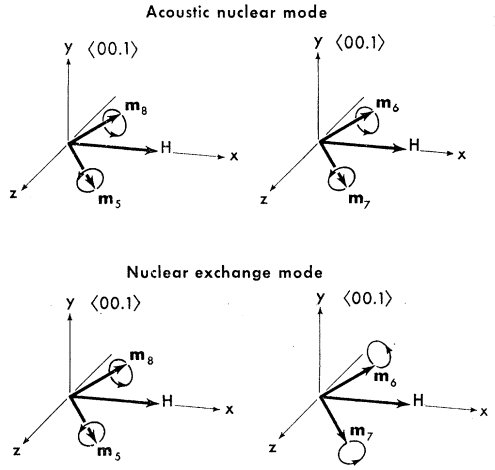

FIG. 3. Diagram of the normal-mode patterns for the acoustic and exchange NMR modes in $CsMnF_3$. The nuclear magnetization $\mathbf{m}_6$ and $\mathbf{m}_7$ are in phase with $\mathbf{m}_5$ and $\mathbf{m}_8$ for the acoustic NMR mode, but they are 180° out of phase with $\mathbf{m}_5$ and $\mathbf{m}_8$ for the exchange NMR mode.

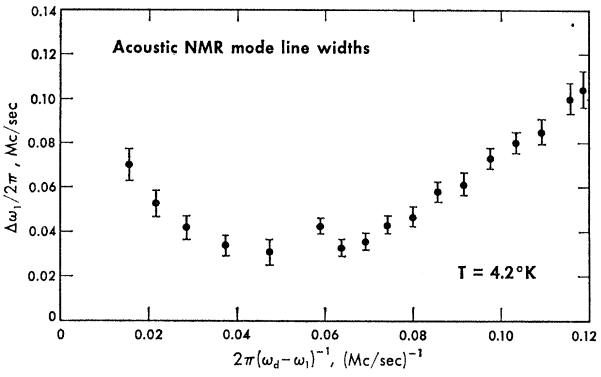

FIG. 4. Dependence of the acoustic NMR mode linewidths on the inverse frequency depression $\delta\nu^{-1}=2\pi(\omega_d-\omega_1)^{-1}$.

Experimental Results

The exchange NMR mode has been observed directly in a single crystal of $CsMnF_3$ using techniques similar to those used in the observation of the acoustic NMR mode. The single crystal of $CsMnF_3$ was supplied by Dr. R. W. H. Stevenson of the University of Aberdeen. The crystal was mounted near the shorted end of a coaxial line. The static and rf fields were applied in the basal plane with the rf field perpendicular to the static field. The observations were made by sweeping the rf frequency through the resonant frequency. The detection system was tuned to the absorptive part of the nuclear resonance by placing the detecting crystal at an electric field maximum. The Q of the detecting system was approximately 50 giving a bandwidth of roughly 10 Mc/sec at the resonant frequency. As the linewidth of the exchange mode was 0.2 Mc/sec, the distortion of the exchange-mode resonance by the Q of the detecting system was negligible. Field modulation and lock-in phase detection were used to give the necessary signal-to-noise ratio.

The exchange-mode NMR signal is much weaker than the acoustic-mode signal. The linewidths of the exchange mode are larger than those of the acoustic mode. At 5000 Oe the exchange-mode linewidth is 0.22 ± 0.03 Mc/sec while the acoustic-mode linewidth is 0.042 ± 0.003 Mc/sec. The exchange-mode linewidth increases with field from ≈0.18 Mc/sec at 2500 Oe to ≈0.4 Mc/sec at 7500 Oe. Within experimental error no variation of the exchange-mode linewidth was observed as the temperature was varied from 1.35 to 4.2°K at fixed field. The field dependence of the acoustic-mode linewidth is more complicated. At fields less than 1000 Oe, the field linewidths of the acoustic NMR mode and the low-lying AFR mode are the same and they increase rapidly as the field is lowered to zero.[10] These linewidths are thought to result from crystal imperfections. The linewidths of the acoustic mode between 2500 and 7000 Oe at 4.2°K are shown in Fig. 4. The linewidth measurements were made using field modulation with lock-in phase detection. The amplitude of the field modulation was small compared to the NMR field linewidth so the derivative of the absorption curve was observed. The linewidths shown in Fig. 4 are the frequency difference of the two peaks plotted as a function of $\delta\nu^{-1}=2\pi(\omega_d-\omega_1)^{-1}$. The shape of the acoustic NMR line was found to be Lorentzian out to more than four linewidths.

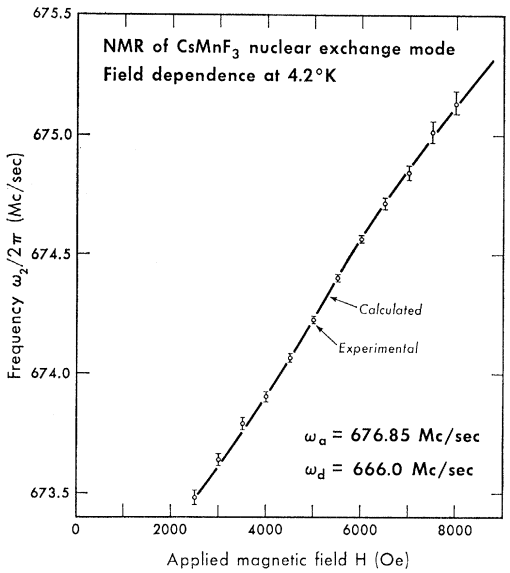

FIG. 5. Field dependence of the Mn^{55} exchange NMR mode at $T=4.2$°K with the applied magnetic field at the basal plane.

The field dependence of the exchange mode for fields between 2500 Oe and 8000 Oe at 4.2°K is shown in Fig. 5. No angular dependence was observed in the basal plane in agreement with the NMR results on the acoustic mode.[4] The temperature dependence of the exchange NMR mode is shown in Fig. 6 for temperatures between 1.35 and 4.2°K at 5000 Oe. Apart from the field dependence of ω_2, the same temperature dependence is observed at other fields within experimental error.

Discussion of Results

The linewidths of both the exchange and acoustic NMR modes are much narrower than the full linewidth of 1.4 Mc/sec predicted for the second moment by the Suhl-Nakamura theory[11,12] using the results of the spin-wave calculations of Sec. III. For $\delta\nu^{-1}$ less than 0.05 (fields less than 4500), the increase in linewidth is thought to result from crystal imperfections which broaden the AFR line and hence the NMR line. For low fields this contribution to the linewidth appears to dominate as discussed elsewhere.[10] For higher applied

[10] L. B. Welsh, thesis, University of California, 1966 (unpublished).

[11] H. Suhl, Phys. Rev. **109**, 606 (1958).

[12] T. Nakamura, Progr. Theoret. Phys. (Kyoto) **20**, 542 (1958).

fields ω_1 becomes less sensitive to variations in the AFR frequency, so the observed linewidths above $\delta\nu^{-1}=0.06$ are probably not affected by crystal imperfections. The behavior of the acoustic-mode linewidth is essentially linear with $\delta\nu^{-1}$ for $\delta\nu^{-1}>0.07$. This indicates the linewidths at very small frequency depressions may be considerably broader than those observed here. Small frequency depressions correspond to very little coupling between nuclear spins and the infinite nuclear temperature approximation should apply.[11,12] It would be interesting to see if a calculation of both the second and fourth moments in the finite-nuclear-temperature approximation could account for the observed linewidths and the Lorentzian line shape.

The field dependence of the exchange NMR mode shown in Fig. 5 can be explained in terms of Eqs. (16) if the hyperfine interaction constant α_a is greater than α_d. Good agreement between the observed NMR frequencies of both modes and Eqs. (16) result with the choice of parameters: $H_E=3.35\pm0.05\times10^5$ Oe, $\omega_a/2\pi=676.85\pm0.1$ Mc/sec, and $\omega_d/2\pi=666.0\pm0.2$ Mc/sec at 4.2°K. This agreement is shown in Fig. 5 for the exchange mode and in Fig. 7 for both the acoustic and exchange modes.

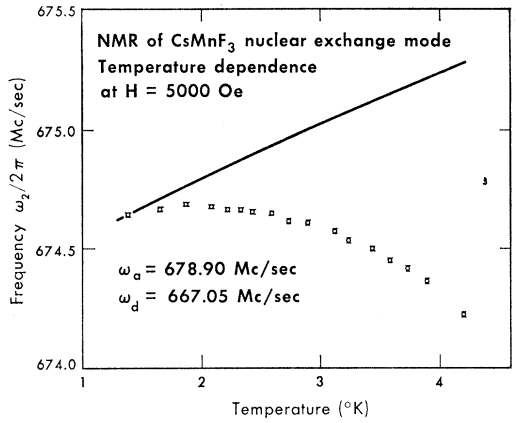

FIG. 6. Temperature dependence of the exchange NMR mode at 5000 Oe with the applied magnetic field in the basal plane. The solid curve is the calculated temperature dependence assuming no temperature variation of the sublattice magnetization.

The values of $\omega_a/2\pi$ and $\omega_d/2\pi$ are lower than the frequencies determined from the free ion hyperfine interaction This reduction is attributable to corrections which must be made for both covalency effects and zero-point spin-wave reductions. Covalency effects may be taken into account by making corrections for the volume of the F^- octahedrons. Estimates of these corrections based on the paramagnetic resonance studies of Ogawa[13] have been made by Lee *et al.*[1] They obtain frequencies of 692±7 Mc/sec for the Mn1 site and 688±7 Mc/sec for the Mn2 site. If the difference between these frequencies and the experimentally determined frequencies is attributed solely to the zero-point spin-wave reduction, the reductions are (2.2±1.0)% for the Mn1 site and (3.2±1.0)% for the Mn2 site. It is interesting to compare these values with the linked-spin-cluster expansion calculations done by Davis.[14] Figure 1 shows the Mn1 sites have six nearest neighbors and the Mn2 sites have four nearest neighbors. Davis calculated his results for several lattices. The simple cubic (sc) lattice best fits the Mn1 site and has a 2.49% reduction. The Mn2 site may be crudely approximated by a planar lattice which has a 4.36% reduction. These reductions are in reasonable agreement with the estimated reductions based on the observed hyperfine interaction constants.

The absorptions of the acoustic and exchange NMR modes may be calculated from the imaginary part of the rf susceptibilities. These are obtained by calculating the response of the nuclear magnetizations to an rf field, assuming no damping. The rf field, **h**, adds the energy

$$U_{\rm rf}=-\mathbf{h}\cdot(\mathbf{m}_5+2\mathbf{m}_6+2\mathbf{m}_7+\mathbf{m}_8)\,, \qquad (18)$$

to the total energy of the nuclei. Equation (18) adds a forcing function involving **h** to the resonance matrix generated by Eqs. (14) and (15). Then χ'' is obtained from χ using the substitutions $\omega_1\rightarrow\omega_1+i\Delta\omega_1$ and $\omega_2\rightarrow\omega_2+i\Delta\omega_2$, where $\Delta\omega_1/2\pi$ and $\Delta\omega_2/2\pi$ are the linewidths of the NMR modes. Since we have $\chi=\chi'-i\chi''$, χ'' can be determined. When the frequency of

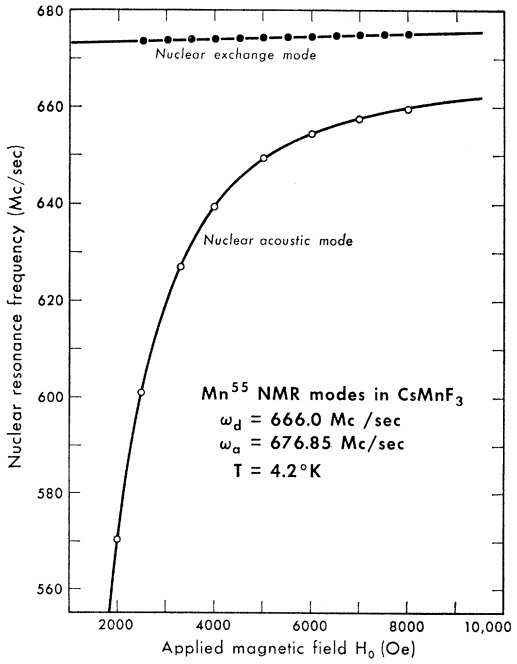

FIG. 7. Field dependence of the exchange and acoustic Mn^{55} NMR modes in $CsMnF_3$ with the applied magnetic field in the basal plane.

[13] S. Ogawa, J. Phys. Soc. Japan **15**, 1475 (1960).

[14] H. L. Davis, Phys. Rev. **120**, 789 (1960).

the rf field is $\omega=\omega_1$ or ω_2, we have

$$\chi_i''(\omega)=m_a\gamma[(\omega^2-\omega_d^2)\epsilon_a\omega_a - \omega_d\gamma H\Gamma^2 4H_E H_{AT_d}/3\Omega_1^2]/Q, \quad i=5,8; \quad (19)$$

$$\chi_i''(\omega)=2m_d\gamma[(\omega^2-\omega_a^2)\epsilon_d\omega_d + \omega_a\gamma H\Gamma^2 2H_E H_{AT_a}/3\Omega_1^2]/Q, \quad i=6,7; \quad (20)$$

where $Q=2\omega_1\Delta\omega_1(\omega_2^2-\omega^2)+2\omega_2\Delta\omega_2(\omega_1^2-\omega^2)$. The absorbed power is $P=\frac{1}{2}\omega\chi''h^2$. Since we have $\omega_2-\omega_1\ll\omega$ at 5000 Oe and the amplitude of the rf field was the same in the observation of both modes, the ratio of the signals is $\sum_i\chi_i''(\omega_1)/\sum_i\chi_i''(\omega_2)$ where the detecting crystal is operated in the square law region. This ratio is 80 at 5000 Oe. Field-modulation techniques were used in the observation of the exchange NMR mode. This requires that the ratio above be multiplied by the factor $3\delta H/(4\Delta H_T)$ for a Lorentzian line where the peak to peak af field amplitude δH is much less than the full linewidth in field ΔH_T. The calculated ratio of the acoustic-mode signal to the exchange-mode signal is roughly 2700 at 5000 Oe assuming both NMR modes have Lorentzian line shapes. Considering the uncertainties in the NMR mode linewidths and in the observed ratio, the calculated and observed ratios are consistent. This result supports the identification of the higher NMR signal with the exchange NMR mode predicted by the four-sublattice model presented here.

The comparison of the temperature dependence data for the exchange NMR mode with the expected behavior calculated from Eqs. (16) is shown in Fig. 6. The temperature dependence of Eq. (16) differs considerably from the observed temperature dependence. This difference is shown in Fig. 8. The exchange and hyperfine constants are normally assumed to remain constant in the paramagnetic and ordered states so the temperature variation of λ and α should be negligible between 1 and 4°K. Since no anisotropies are involved in the AFR mode Ω_1, the only temperature-dependent

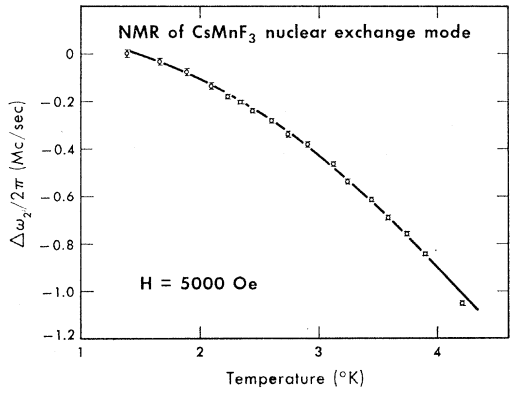

FIG. 8. Deviation of the observed Mn^{55} exchange NMR frequency temperature dependence from the computed temperature-dependence assuming the sublattice magnetization is temperature-independent. The solid curve is the computed deviation obtained from electron spin-wave calculations.

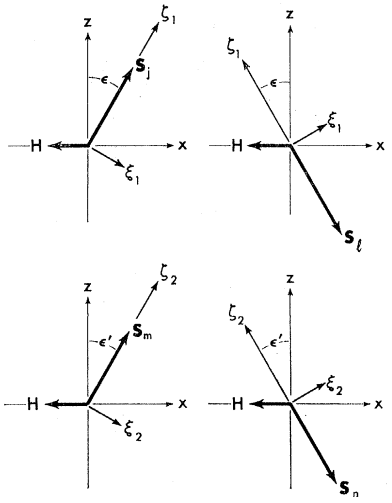

FIG. 9. The ξ, η, ζ coordinate systems for the electron spins.

quantities in Eqs. (16) are H_{AT}, ω_a, and ω_d. The temperature dependence of ω_a and ω_d results from their dependence on the sublattice magnetization. If the assumption is made that the variation of the sublattice magnetization with temperature is the same for Mn1 sites and Mn2 sites, the changes in ω_a and ω_d with temperature will be the same. Then as long as the static field is large, the variation of the exchange NMR frequency $\omega_2/2\pi$ equals the variation of $\omega_a/2\pi$ and $\omega_d/2\pi$ to within 0.1%. The above assumption will be considered in the next section where a calculation of the temperature dependence of the sublattice magnetization is described.

III. TEMPERATURE DEPENDENCE OF THE SUBLATTICE MAGNETIZATION

In order to calculate the temperature dependence of the sublattice magnetization, the electron spin-wave spectrum and the spin-wave amplitudes must be known. These may be calculated from the total energy of the electron spin system. In terms of the spin variables the electronic part of Eq. (5) is

$$\mathcal{H}=2J_1(\sum_{j,n}\mathbf{S}_j\cdot\mathbf{S}_n+\sum_{l,m}\mathbf{S}_l\cdot\mathbf{S}_m)+2J_2\sum_{n,m}\mathbf{S}_n\cdot\mathbf{S}_m - \Gamma\hbar H(\sum_j S_j^x+\sum_l S_l^x+\sum_m S_m^x+\sum_n S_n^x) + K'(\sum_j S_j^{y^2}+\sum_l S_l^{y^2}+\sum_m S_m^{y^2}+\sum_m S_n^{y^2}) - K_n(\sum_j S_j^{\xi_1^2}+\sum_l S_l^{\xi_1^2}+\sum_m S_m^{\zeta_2^2}+\sum_n S_n^{\zeta_2^2}). \quad (21)$$

The spins $\mathbf{S}_j$, $\mathbf{S}_l$, $\mathbf{S}_m$, and $\mathbf{S}_n$ are associated with the sublattices $A(+)$, $A(-)$, $D(+)$, and $D(-)$, respectively, so there are twice as many $\mathbf{S}_m$ and $\mathbf{S}_n$ spins as $\mathbf{S}_j$ and $\mathbf{S}_l$ spins; K_n represents the nuclear-induced anisotropy; x, y, z are the crystalline axes oriented such that the y axis is along the crystalline c axis as shown in Fig. 2. The static magnetic field is applied in the negative x direction for this calculation. The electron

spins are tilted from the z axes through the angles ϵ and ϵ' which are given by the equilibrium conditions [Eqs. (6)]. The axes of quantization of the electron spins $\mathbf{S}_j$, $\mathbf{S}_l$, $\mathbf{S}_m$, and $\mathbf{S}_n$ are ζ_1, $-\zeta_1$, ζ_2, and $-\zeta_2$, respectively. Equation (21) is rewritten in terms of the tilted coordinate systems shown in Fig. 9: ξ_1, η_1, ζ_1 for $\mathbf{S}_j$; ξ_1, η_1, $-\zeta_1$ for $\mathbf{S}_l$; ξ_2, η_2, ζ_2 for $\mathbf{S}_m$; and ξ_2, η_2, $-\zeta_2$ for $\mathbf{S}_n$ as described by Keffer and Oguchi.[15]

Using the Holstein-Primakoff transformation to spin-wave variables,[16] the Hamiltonian is reduced to

$$\begin{aligned}\mathcal{H}=\sum_{k>0} & A(a_k^\dagger a_k+a_{-k}^\dagger a_{-k}+b_k^\dagger b_k+b_{-k}^\dagger b_{-k})+B(c_k^\dagger c_{-k}+c_{-k}^\dagger c_{-k}+d_k^\dagger d_k+d_{-k}^\dagger d_{-k})+C(a_k a_{-k}+a_k^\dagger a_{-k}^\dagger \\ & +b_k^\dagger b_{-k}^\dagger+b_k b_{-k}+c_k c_{-k}+c_k^\dagger c_{-k}^\dagger+d_k^\dagger d_{-k}^\dagger+d_k d_{-k})+D(a_k d_{-k}^\dagger+a_{-k} d_k^\dagger+b_k^\dagger c_{-k}+b_{-k}^\dagger c_k+a_k^\dagger d_{-k} \\ & +a_{-k}^\dagger d_k+b_k c_{-k}^\dagger+b_{-k} c_k^\dagger)+E(a_k d_k+a_{-k} d_{-k}+b_k^\dagger c_k^\dagger+b_{-k}^\dagger c_{-k}^\dagger+a_k^\dagger d_k^\dagger+a_{-k}^\dagger d_{-k}^\dagger+b_k c_k+b_{-k} c_{-k}) \\ & +D'(c_k d_{-k}^\dagger+c_{-k} d_k^\dagger+c_k^\dagger d_{-k}+c_{-k}^\dagger d_k)+E'(c_k d_k+c_{-k} d_{-k}+c_k^\dagger d_k^\dagger+c_{-k}^\dagger d_{-k}^\dagger), \quad (22)\end{aligned}$$

where

$$\begin{aligned}A&=[2J_1SZ\cos(\epsilon+\epsilon')+\Gamma\hbar H\sin\epsilon+K'S+2SK_n],\\ B&=[J_1SZ\cos(\epsilon+\epsilon')+2J_2S\cos(2\epsilon')\\ &\quad+\Gamma\hbar H\sin\epsilon'+K'S+2SK_n],\\ C&=-SK',\\ D&=J_1SZ\gamma_j[\cos(\epsilon+\epsilon')-1]/\sqrt{2},\\ D'&=J_2S\gamma_n[\cos(2\epsilon')-1],\\ E&=J_1SZ\gamma_j[\cos(\epsilon+\epsilon')+1]/\sqrt{2},\\ E'&=J_2S\gamma_n[\cos(2\epsilon')+1],\end{aligned} \quad (23)$$

and a, b, c, and d are the operators for the sublattices 1, 4, 3, and 2, respectively. The γ factors are given by

$$\gamma_j=\frac{1}{Z}\sum_{\delta_{12}} e^{i\mathbf{k}\cdot\delta_{12}}=1-a_1^2k^2(\sin^2\theta)/4-a_2^2k^2(\cos^2\theta)/2, \quad (24)$$

$$\gamma_n=\cos\mathbf{k}\cdot\boldsymbol{\delta}_{22}=1-a_3^2k^2(\cos^2\theta)/2, \quad (25)$$

in the long-wavelength approximation; θ is measured from the c axis. The vectors $\boldsymbol{\delta}_{12}$ are the vectors from one Mn1 site to its Z nearest neighbors in Mn2 sites. The vector $\boldsymbol{\delta}_{22}$ is from one Mn2 site to its nearest neighbor Mn2 site; a_1 is the projection of the Mn1-Mn2 distance in the basal plane; a_2 is the projection of the Mn1-Mn2 on the c axis; a_3 is the distance between the Mn2 sites; $a_1=3.58$ Å, $a_2=2.27$ Å, and $a_3=3.00$ Å.

The spin-wave spectrum and amplitudes of Eq. (22) can be obtained using the techniques of White *et al.*[17] Equation (22) is rewritten in the form

$$\mathcal{H}=\mathbf{X}^\dagger\mathbf{H}\mathbf{X}, \quad (26)$$

where

$$\mathbf{X}^\dagger=(a_k^\dagger a_{-k} d_{-k}^\dagger d_k b_{-k}^\dagger b_k c_k^\dagger c_{-k}). \quad (27)$$

The transformation which diagonalizes (26) is

$$\mathbf{X}=\mathbf{S}\mathbf{X}', \quad (28)$$

where

$$\mathbf{X}'^\dagger=(\alpha_k^\dagger\alpha_{-k}\beta_{-k}^\dagger\beta_k\chi_{-k}^\dagger\chi_k\sigma_k^\dagger\sigma_{-k}). \quad (29)$$

The calculations of the eigenvalues and of the elements of the matrix $\mathbf{S}$ are considered elsewhere.[10] Four branches of the spin-wave spectrum result which for $\mathbf{k}=0$ are identical to the AFR modes of Eqs. (9) through (12). The energies of magnons in the two exchange modes (11) and (12) are of order $\hbar\Gamma H_E\approx k_B\times 60°\mathrm{K}$. The energy of magnons in mode (10) are of order $\Gamma\hbar(2H_EH_A)^{1/2}\approx k_B\times 12°\mathrm{K}$ for $\mathbf{k}=0$. Since the experiments discussed here were performed in the temperature range of 1.35 to 4.2°K, the populations of the spin-wave modes in the upper three branches will be negligible. Only results for the low-frequency spin-wave branch (α) need be considered here. Figure 10 shows the computed spin-wave spectrum $\Omega_1(\mathbf{k})/2\pi$ versus $\mathbf{k}$ for $\mathbf{k}$ both perpendicular and parallel to the c axis at 5000 Oe, at 4.2°K, and with $\lambda_1=\lambda_2$. The spectrum is anisotropic. For a given wavelength, the frequency of the spin-wave mode is lower if $\mathbf{k}$ is perpendicular to the c axis. The anisotropy in the spectrum as a function

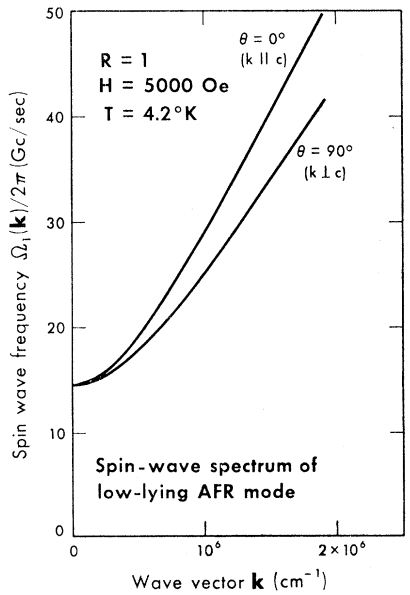

FIG. 10. Computed spin-wave spectrum of the low-lying branch for $\mathbf{k}$ perpendicular and parallel to the hexagonal c axis and for $R=1$.

[15] T. Oguchi and F. Keffer, J. Phys. Chem. Solids **25**, 405 (1964).
[16] T. Holstein and H. Primakoff, Phys. Rev. **58**, 1098 (1940).
[17] R. M. White, M. Sparks, and I. Ortenburger, Phys. Rev. **139**, A450 (1965).

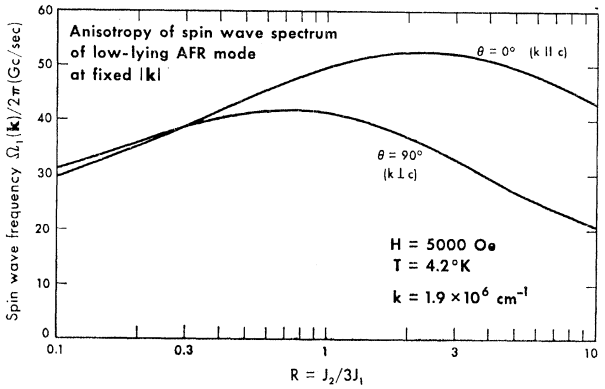

FIG. 11. Anisotropy of the spin-wave spectrum of the low-lying branch as a function of R for fixed $|\mathbf{k}|$.

of $R=\lambda_2/\lambda_1=J_2/3J_1$ is shown in Fig. 11 by plotting the values of $\Omega_1(\mathbf{k})/2\pi$ for both $\theta=0°$ and $\theta=90°$ with fixed $|\mathbf{k}|$. The uniform mode is held constant as a function of R by requiring J_2+3J_1 be constant. The spectrum is nearly isotropic for $R<1$ but anisotropic for $R>1$. The spin-wave amplitudes (the elements of $\mathbf{S}$) are proportional to $[\Omega_1(\mathbf{k})]^{1/2}$. The proportionality constants are a maximum when $R=1$.

The effects of dipolar fields have been neglected in the above calculation. These effects have been discussed by several authors.[18,19] They show that the dipolar effects are proportional to $\mathbf{k}\cdot\mathbf{M}_\perp$, where $\mathbf{M}_\perp$ is the amplitude of the spin wave. For the $\Omega_1(\mathbf{k})$ branch the spin-wave modes are, in effect, linearly polarized in the basal plane for low $\mathbf{k}$. The effective anisotropy field for the spin waves of this branch is $H_{AT}+H_\epsilon$ for $\lambda_1=\lambda_2$. Referring to the paper by Harris[19] we expect the dipolar interactions to cause an increase in the exchange constant by $4\pi M$ or 0.2% ($M=13\,850$ emu/mole) and an additional anisotropy in $\Omega_1(\mathbf{k})$ of order $\Gamma^2(H_{AT}+H_\epsilon)\times 4\pi M_S/\Omega_1(\mathbf{k})\approx 2\%$. Both of these effects are negligible.

The spin-wave dispersion relation may be written in the form

$$\Omega_1(\mathbf{k})=(\Omega_g^2+\alpha^2k^2\sin^2\theta+\beta^2k^2\cos^2\theta)^{1/2}. \quad (30)$$

For low $\mathbf{k}$ the square of the spin-wave amplitudes may be written as

$$S_{ij}^2=K_{ij}^2/\Omega_1(\mathbf{k}), \quad (31)$$

where α, β, and K_{ij} are determined from the results of the calculations described above and are functions of R. Using Eqs. (30) and (31) the temperature dependences of ω_a and ω_d can be calculated. The temperature dependence of ω_a is

$$\Delta\omega_a(T)/2\pi=(A/h)\textstyle\sum_{\mathbf{k}} a_{\mathbf{k}}^\dagger a_{\mathbf{k}}/N, \quad (32)$$

$$=(A/h)\textstyle\sum_{\mathbf{k}}(S_{11}^2+S_{12}^2)\langle\alpha_{\mathbf{k}}^\dagger\alpha_{\mathbf{k}}\rangle/N. \quad (33)$$

The sum can be converted to the integral

$$\Delta\omega_a(T)/2\pi=[A(K_{11}^2+K_{12}^2)/h]\times\int_{\Omega_g}^{\Omega_{\max}}\frac{N(\Omega)d\Omega}{\Omega(e^{\hbar\Omega/kBT}-1)}, \quad (34)$$

where $\Omega_g/2\pi$ is the uniform mode frequency and $\Omega_{\max}/2\pi$ is the frequency at the zone boundary. The density of spin-wave states for the single branch $\Omega_1(\mathbf{k})$ is

$$N(\Omega)=\frac{v_c}{(2\pi)^3}\frac{dV_k}{d\Omega}=\frac{v_c}{2\pi^2}\frac{\Omega(\Omega^2-\Omega_g^2)^{1/2}}{\alpha^2\beta}, \quad (35)$$

where V_k is the volume of k space about $\mathbf{k}=0$, and v_c is the volume of the unit cell ($v_c=5.0\times10^{-22}$ cm^3). Making the substitution $x=\hbar\Omega/k_BT$ in the integral, the temperature dependence of $\Delta\omega_a/2\pi$ is

$$\frac{\Delta\omega_a(T)}{2\pi}=\Lambda T^2\int_{x_g}^{x_{\max}}\frac{(x^2-x_g^2)^{1/2}}{e^x-1}dx \quad (36)$$

where

$$\Lambda=Ak_B^2v_c(K_{11}^2+K_{12}^2)/(2\pi^2\hbar\hbar^2\alpha^2\beta). \quad (37)$$

The solid curve of Fig. 8 is for $\Lambda=0.048$ Mc/sec. Equation (37) gives $\Lambda=0.129$, 0.108, and 0.226 Mc/sec for $R=0.1$, 1, and 10, respectively. The value of Λ from Eq. (37) is fairly insensitive to R and larger than the resonance value of Λ for all R. The calculation for $\Delta\omega_d/2\pi$ gives the same temperature dependence.

Agreement between the theoretical calculations for this model and the experimental results may be obtained by introducing ferromagnetic next-nearest-neighbor (nnn) exchange within the sublattices. The most likely path of exchange would be Mn-F-F-Mn, where the fluorine and manganese ions belong to neighboring octahedra. Since this exchange occurs in the basal plane, the spin-wave frequencies of modes with $\mathbf{k}$ parallel to the c axis will not be affected. The total

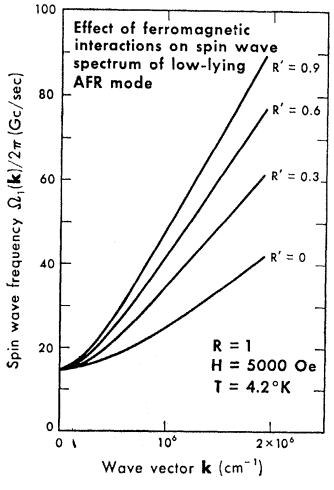

FIG. 12. Effect of the ferromagnetic intra-sublattice interactions on the spin-wave spectrum of the low-lying branch for $R=1$.

[18] R. Loudon and P. Pincus, Phys. Rev. **132**, 673 (1963).
[19] A. Brooks Harris, Phys. Rev. **143**, 353 (1966).

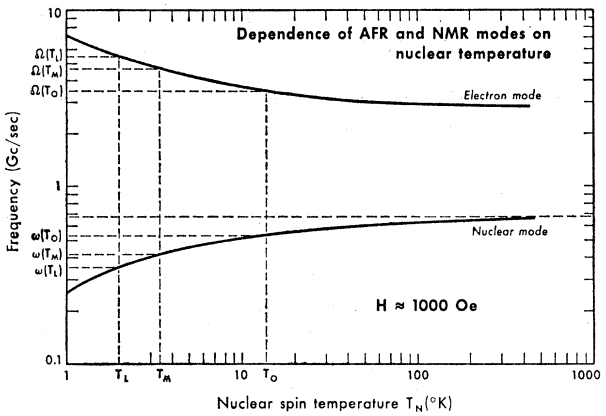

FIG. 13. Dependence of the AFR and acoustic NMR modes on the nuclear spin temperature at fixed applied magnetic field.

energy of the electron system is changed by

$$\Delta U=-2J'(\sum_{j,j'}\mathbf{S}_j\cdot\mathbf{S}_{j'}+\sum_{l,l'}\mathbf{S}_l\cdot\mathbf{S}_{l'}+\sum_{m,m'}\mathbf{S}_m\cdot\mathbf{S}_{m'}+\sum_{n,n'}\mathbf{S}_n\cdot\mathbf{S}_{n'}). \quad (38)$$

As this is an intrasublattice interaction, neither the equilibrium positions of the sublattices nor the uniform mode resonance frequencies will be affected. In Eqs. (23), A and B are modified by the addition of the term $4J'SZ'(1-\gamma')$, where the number of next-nearest neighbors is $Z'=6$, and $\gamma'=1-a^2k^2(\sin^2\theta)/4$. The resulting modification of $\Omega_1(\mathbf{k})$ for $R=1$ is shown in Fig. 12 for several values of R'. The parameter $R'=2J'/J_1$ is the ratio of the intra-sublattice ferromagnetic exchange constant to the intersublattice antiferromagnetic exchange constant. Agreement between the theoretical and experimental values of Λ can be obtained when R' is 0.32. The actual value of R is uncertain so this value of R' is only approximate. But since Λ is relatively insensitive to R and is quite sensitive to R', the value of R' will not vary greatly over the range of R.

Incomplete susceptibility measurements in the paramagnetic region obtained by Lee *et al.*[1] indicate the paramagnetic constant θ is of the order of 55°K. In terms of the two-sublattice model, ferromagnetic nnn exchange lowers θ. Then $\theta=C(\lambda_1-\lambda')$, where C is the Curie constant and λ' is the ferromagnetic exchange constant. The θ we obtain is 36°K. It would be useful to have a complete set of susceptibility measurements in the paramagnetic region in order to determine θ accurately.

The four-sublattice model of $CsMnF_3$ described here accounts for the presence and observed behavior of the exchange NMR mode. The temperature dependence of the exchange NMR mode allows the temperature dependence of the sublattice magnetization to be determined. The spin-wave calculation based on the four-sublattice model can account for the observed temperature dependence of the sublattice magnetization when intrasublattice ferromagnetic exchange is included.

IV. NUCLEAR SPIN-LATTICE RELAXATION

Theory

Because of the strong coupling of the low-lying AFR mode with the NMR modes, the frequencies of these modes are strongly dependent on the nuclear temperature, T_N. Figure 13 shows this dependence for the low-lying AFR mode and the acoustic NMR mode calculated from Eqs. (9) and (16) at fixed field. This dependence on T_N allows the study of nuclear spin-lattice relaxation by monitoring the recovery of either the AFR mode or the acoustic NMR mode. If the nuclear spin system is in equilibrium with the lattice, $T_N=T_L$ where T_L is the lattice temperature. The corresponding AFR and NMR frequencies are $\Omega(T_L)/2\pi$ and $\omega(T_L)/2\pi$. Because of the existence of crystalline imperfections it is possible to partially saturate the nuclei at a frequency, $\omega(T_0)/2\pi$, between $\omega(T_L)/2\pi$ and $\gamma\alpha M/2\pi$[1] (See Fig. 13). This absorption of rf power off resonance has been discussed by Witt and Portis[2] in terms of a spin-pinning model. Applying rf power at $\omega(T_0)/2\pi$ heats the nuclei to the temperature T_0 and lowers the AFR frequency to $\Omega(T_0)/2\pi$. The relaxation measurements are made by monitoring the AFR or NMR signal at several intermediate frequencies $\Omega(T_M)/2\pi$ or $\omega(T_M)/2\pi$ and measuring the elapsed time between turning the rf power at $\omega(T_0)/2\pi$ off and the appearance of an AFR or NMR signal at the intermediate frequency.

The relaxation of the nuclear magnetization to equilibrium is assumed to be exponential so that we have

$$dm(T_N)/dt=-[m(T_N)-m(T_L)]/T_1. \quad (39)$$

At time $t=0$, $T_N=T_0$. Then at time t_M, the nuclear spins have relaxed to the temperature $T_N=T_M$. If the assumption is made that $\Gamma H\gg\omega(T_L)$, then for the relations between the monitoring frequencies and the elapsed time, t_M, at fixed field we have

$$[1/\omega(T_L)^2-1/\omega(T_M)^2]/[1/\omega(T_L)^2-1/\omega(T_0)^2]=\exp[-t_M/T_1], \quad (40)$$

when the NMR signal is monitored, and we have

$$[\Omega(T_L)^2-\Omega(T_M)^2]/[\Omega(T_L)^2-\Omega(T_0)^2]=\exp[-t_M/T_1], \quad (41)$$

when monitoring the AFR signal.

Experimental Results

The relaxation of the acoustic NMR mode was observed by switching between two coaxial circuits. One circuit providing power in excess of 10 W at the frequency $\omega(T_0)/2\pi$ partially saturates the nuclei at $T_0>T_L$. In times of the order of ten milliseconds the

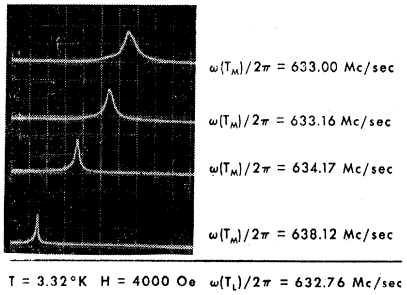

FIG. 14. Sample traces of the relaxation of the acoustic NMR signal for several different monitoring frequencies.

shorted coaxial line containing the $CsMnF_3$ crystal was switched from this circuit to the second coaxial circuit. This circuit monitors the acoustic NMR signal at the frequency $\omega(T_M)/2\pi$. The output of the detecting diode was fed into a high dc-gain oscilloscope. Using the turn-off of the rf power to trigger the oscilloscope, traces of the type shown in Fig. 14 were obtained as the monitoring frequency was varied. As $\omega(T_M)/2\pi$ approaches $\omega(T_L)/2\pi$, the NMR signal takes longer to appear at $\omega(T_M)/2\pi$ and is also broader in time since the frequency of the resonance is changing more slowly with time. At the lowest temperatures "capture" of the NMR line at $\omega(T_M)/2\pi$ occurred if the monitoring power level was too high. Monitoring power levels were lowered until no effect upon the traces was detected by further reduction.

The monitor circuit could be used at microwave frequencies with the addition of waveguide-to-coaxial line adapters. This allowed similar data to be obtained by monitoring the AFR signal. This type of experiment is very similar to the transient electron-nuclear-double-resonance experiments described by Witt and Portis.[2]

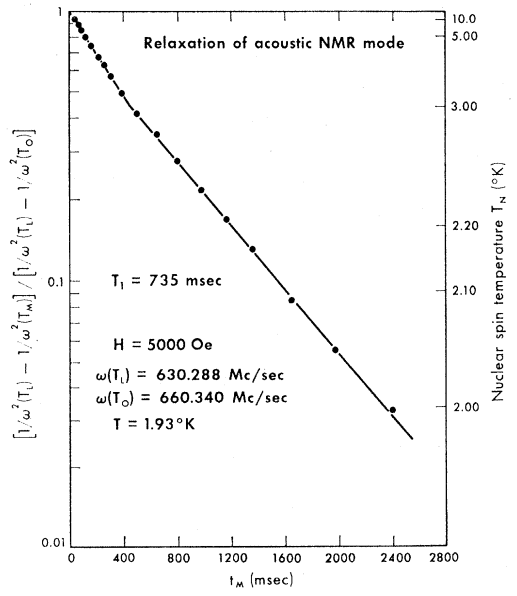

FIG. 15. Determination of the Mn^{55} spin-lattice relaxation time by monitoring the acoustic NMR mode after partial saturation. The inverse relaxation time $1/T_1$ is obtained from the slope of the solid curve.

Figure 15 shows the relaxation of the acoustic mode to its equilibrium value $\omega(T_L)/2\pi$ for $T_L=1.93$°K and $H=5000$ Oe. The relaxation of the nuclear magnetization T_0 to T_M for T_M close to T_0 is governed by a somewhat faster relaxation time than when T_M is close to T_L. In what follows, the relaxation times referred to are those for T_N within 1 deg of the lattice temperature. In this region the relaxation is definitely exponential. The field dependence of the relaxation time is plotted in Fig. 16 for fields between 600 and 5000 Oe at 4.2°K. The temperature dependence of the relaxation times between 1.35°K and 4.2°K is plotted in Fig. 17 for an applied field of 5000 Oe. For this field $T_1 \propto T^{-4.96\pm0.03}$. Temperature dependences at lower fields give a power

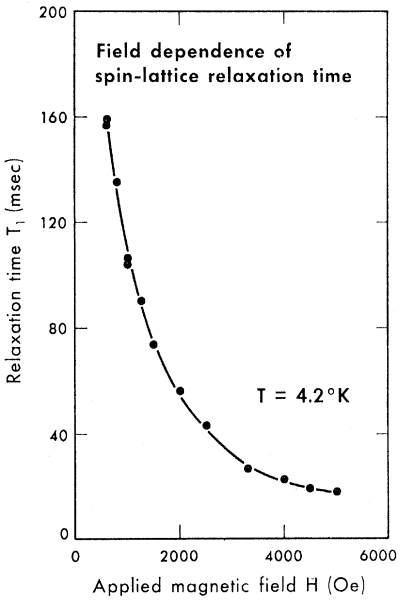

FIG. 16. Field dependence of the Mn^{55} spin-lattice relaxation time at 4.2°K.

law which varies more slowly ($T^{-4.60}$ for the temperature dependence at 1500 Oe).

It is also possible to use the exchange NMR mode in relaxation experiments. The steady-state electron-nuclear-double-resonance experiments of Lee *et al.*[1] show that the nuclei can be partially saturated when rf power is supplied at exchange-mode frequencies. The powers needed to obtain a partial saturation of the exchange mode are comparable to those needed to obtain a complete shift of the NMR and AFR lines by partial saturation of the acoustic mode. The shifts obtained through the excitation of the exchange mode are very power-dependent and are probably the result of the direct absorption of energy in the wings of the line. Figure 18 shows the relaxation of the acoustic mode at 4.2°K and 3300 Oe with the rf power supplied at 676.78 Mc/sec. This relaxation curve extrapolates to an effective $\omega(T_0')/2\pi$ for the acoustic mode of 648

Mc/sec which corresponds to $T_0'=8.5°K$. The same relaxation times are obtained whether the nuclear spin system is excited through the exchange NMR mode or the acoustic NMR mode.

Discussion of Results

These relaxation times are considerably longer than those observed by Witt and Portis[2] on samples prepared by Lee. Their data were obtained using electron-nuclear double resonance techniques. At the same applied fields their data show a T^{-2} temperature dependence and at 2°K are more than an order of magnitude faster. In order to insure that the direct observation of the NMR signal and the double resonance method give the same results, the relaxation of the AFR signal was studied at X-band frequencies. The relaxation times obtained by these two methods agree within experimental error as shown in Fig. 19; the temperature dependence of the relaxation times at 3300 Oe. The relaxation times observed by Witt and Portis are believed to be the result of magnetic impurities. These impurities may also be responsible for the weak sixfold anisotropy in the basal plane observed by Lee *et al.*[1] in their samples. Minkiewicz and Nakamura[4] estimated the amount of the Fe^{2+} ion needed to give this anisotropy was of the order of 0.04%. As noted above, the NMR and AFR experiments on the $CsMnF_3$ sample obtained from Stevenson show no sixfold anisotropy.

At present the spin-lattice relaxation times reported here have not been explained theoretically. Using the temperature dependence of the relaxation as the key to its origin, three-magnon processes would seem to be the reasonable explanation. Three-magnon calculations of the relaxation times have been performed.[10] The transverse part of the hyperfine interaction is expanded in the electronic spin-wave creation and annihilation operators and only the terms involving three spin-wave operators are kept. Using the computed spin-wave spectrum for $CsMnF_3$, these calculations give a temperature dependence of $T_1 \propto T^{-5.4}$ at 5000 Oe and a dependence of $T_1 \propto T^{-5.1}$ at 1500 Oe. However these calculations do not account for the field dependence of T_1 and result in relaxation times which are 10^3 too long. These calculations have not considered the exchange-scattering correction discussed by Pincus[20] which may

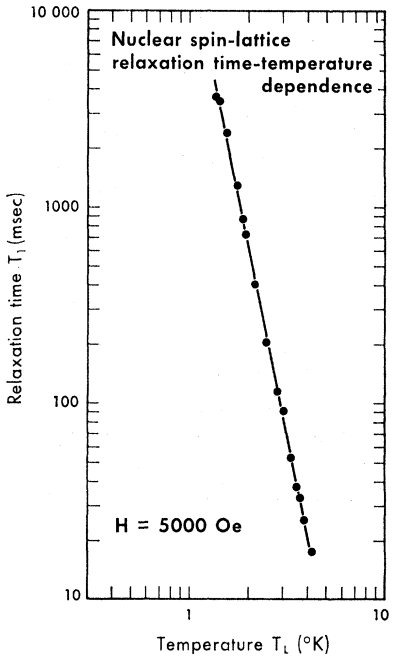

FIG. 17. Temperature dependence of the Mn^{55} spin-lattice relaxation time for an applied magnetic field of 5000 Oe.

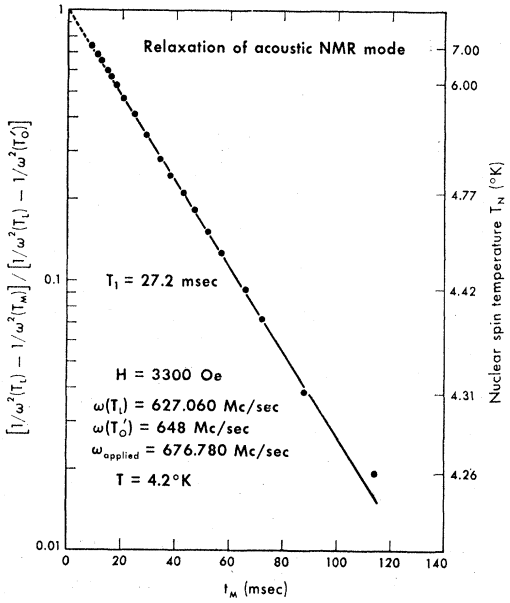

FIG. 18. Determination of the Mn^{55} spin-lattice relaxation time for nuclear excitation through the exchange NMR mode. The acoustic NMR mode is monitored. The relaxation times obtained this way agree with those obtained when the nuclei are excited through the acoustic NMR mode.

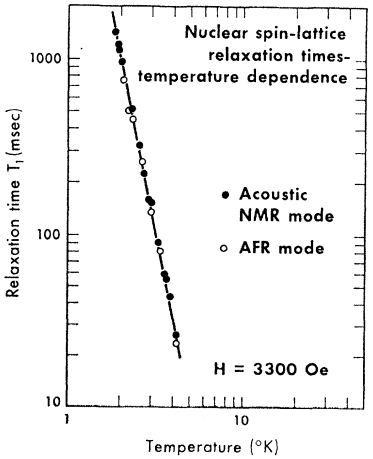

FIG. 19. Comparison of the Mn^{55} spin-lattice relaxation times obtained by monitoring the acoustic NMR mode directly with those obtained using electron-nuclear double resonance where the AFR mode is monitored.

[20] P. Pincus, Phys. Rev. Letters **16**, 398 (1966).

be as large as a factor of ten (which would reduce the disagreement to a factor of 10^2).

Summary

The four-sublattice model of $CsMnF_3$ presented here predicts that the exchange NMR mode, in which the neighboring nuclear spins oscillate 180° out of phase, will be observable when the hyperfine interaction constants differ for the Mn1 and the Mn2 sites. This exchange NMR mode has been observed directly. These observations show the Mn1 sites have the stronger hyperfine coupling which is $\omega_a/2\pi = A(\text{Mn1}) \times \langle S \rangle/h = 676.85 \pm 0.1$ Mc/sec while the coupling for the Mn2 sites is $\omega_d/2\pi = A(\text{Mn2})\langle S \rangle/h = 666.0 \pm 0.2$ Mc/sec. The zero-point reductions for the electron spins are estimated to be $2.2 \pm 1.0\%$ for the Mn1 site and $3.2 \pm 1.0\%$ for the Mn2 site. These reductions are in reasonable agreement with theory.

The temperature dependence of the sublattice magnetization has been determined from the temperature dependence of the exchange NMR mode on the basis of the four-sublattice model of $CsMnF_3$. Electron spin-wave calculations based on the four-sublattice model of $CsMnF_3$ are also discussed. The lowest branch of the spin-wave spectrum is shown to be nearly isotropic when Mn2-Mn2 coupling is of the order of the Mn1-Mn2 coupling ($R<1$), but is anisotropic when the Mn2-Mn2 coupling is much larger than the Mn1-Mn2 coupling ($R>1$). Agreement of the measured temperature dependence of the sublattice magnetization with that calculated from the computed spin-wave spectrum can be obtained when ferromagnetic intrasublattice coupling is included which is equal to 32% of the intersublattice antiferromagnetic coupling (assuming $R=1$).

The observed linewidths of both the acoustic and exchange NMR modes are considerably narrower than those calculated from the Suhl-Nakamura theory using the results of the spin-wave calculation presented here. This theory gives a full linewidth of 1.4 Mc/sec. This is more than a factor of 10 broader than the observed full linewidth of the acoustic NMR mode which is 0.042 Mc/sec at 5000 Oe and 4.2°K. This discrepancy may result from the use of the infinite nuclear temperature approximation in calculating the second and the fourth moments of the Suhl-Nakamura interaction.

The spin-lattice relaxation times of the Mn^{55} nuclear spins have been determined. Assuming the electron and nuclear spins to be coupled by the hyperfine interaction $A\mathbf{I}\cdot\mathbf{S}$, the temperature dependence of the relaxation times is $T_1 \propto T^{-4.96 \pm 0.03}$ at 5000 Oe. This is indicative of three-magnon processes where $T_1 \propto T^{-5.4}$ at 5000 Oe. However the observed relaxation times at 5000 Oe range from 17 msec at 4.2°K to 3.7 sec at 1.4°K, and they are faster than the calculated relaxation times by a factor of 10^3. Furthermore, three-magnon processes do not account for the observed field dependence of the relaxation times. Thus, although the coupling mechanism between the electron and nuclear spins is not understood, three-magnon processes seem to be responsible for the observed relaxation times.

ACKNOWLEDGMENTS

I would like to express my graditude to Professor Alan Portis under whose guidance this research has been carried out. His continued interest and many helpful suggestions have aided considerably in the completion of this work. I would also like to thank Dr. R. M. White for several enlightening discussions.

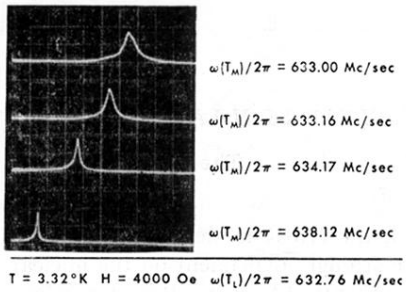

FIG. 14. Sample traces of the relaxation of the acoustic NMR signal for several different monitoring frequencies.